

Effect of Phosphorus Modulation in Iron Single-Atom Catalysts for Peroxidase Mimicking

Shichao Ding, Jordan Alycia Barr, Zhaoyuan Lyu,* Fangyu Zhang, Maoyu Wang, Peter Tieu, Xin Li, Mark H. Engelhard, Zhenxing Feng, Scott P. Beckman, Xiaoqing Pan, Jin-Cheng Li, Dan Du, and Yuehe Lin*

Fe–N–C single-atom catalysts (SACs) exhibit excellent peroxidase (POD)-like catalytic activity, owing to their well-defined isolated iron active sites on the carbon substrate, which effectively mimic the structure of natural peroxidase's active center. To further meet the requirements of diverse biosensing applications, SAC POD-like activity still needs to be continuously enhanced. Herein, a phosphorus (P) heteroatom is introduced to boost the POD-like activity of Fe–N–C SACs. A 1D carbon nanowire (FeNCP/NW) catalyst with enriched Fe–N₄ active sites is designed and synthesized, and P atoms are doped in the carbon matrix to affect the Fe center through long-range interaction. The experimental results show that the P-doping process can boost the POD-like activity more than the non-P-doped one, with excellent selectivity and stability. The mechanism analysis results show that the introduction of P into SAC can greatly enhance POD-like activity initially, but its effect becomes insignificant with increasing amount of P. As a proof of concept, FeNCP/NW is employed in an enzyme cascade platform for highly sensitive colorimetric detection of the neurotransmitter acetylcholine.

peroxidase-like (POD-like) characteristics, which are named Fe–N–C-based single-atom nanozymes (SANs).^[4,5] They can lower the energy barrier of producing reactive intermediates and ultimately catalyze the reduction of H₂O₂ to H₂O.^[6] Two structural features endow Fe-based SACs with outstanding POD-like activity. One is that single-atom engineering can be employed to downsize the metal particles into a low-coordinated metal atom, thereby enhancing the intrinsic catalytic efficiency of each metal atom.^[7] The another is that the Fe–N_x active sites in Fe–N–C-based SACs can mimic the active center of natural horseradish peroxidase (HRP), further increasing the catalytic specificity.^[8,9] Hence, their stable POD-like activity allows them to replace natural enzymes and is widely used in various biosensing processes, including electrochemical biosensors, enzyme cascade reactions, immunoassays, and so

1. Introduction

The precise design of single-atom catalysts (SACs) with isolated active sites at the atomic level has aroused widespread interest due to their homogeneous active sites, exceptional catalytic activity, satisfactory stability, maximum metal atom utilization, and unique geometric structure.^[1–3] Recently, some SACs, particularly Fe-based SACs with isolated Fe atoms, have shown superior

on.^[10,11] For example, our group developed a SAC with high-density Fe–N_x sites that can substitute HRP in a commercial enzyme-linked immunosorbent assay and greatly improved the sensitivity of early stage detection of Alzheimer's disease.^[12] Nevertheless, the intrinsic activity of the current Fe–N–C-based SAC is still inferior to natural enzymes. Massive efforts must be made to continuously improve their catalytic performance to fulfill the high sensitivity requirements of biosensing.

S. Ding, J. A. Barr, Z. Lyu, X. Li, S. P. Beckman, J.-C. Li, D. Du, Y. Lin
 School of Mechanical and Material Engineering
 Washington State University
 Pullman, WA 99164, USA
 E-mail: zhaoyuan.lyu@wsu.edu; yuehe.lin@wsu.edu

F. Zhang
 Department of NanoEngineering and Chemical Engineering Program
 University of California, San Diego
 La Jolla, CA 92093, USA

 The ORCID identification number(s) for the author(s) of this article can be found under <https://doi.org/10.1002/adma.202209633>.
 © 2023 The Authors. Advanced Materials published by Wiley-VCH GmbH. This is an open access article under the terms of the Creative Commons Attribution License, which permits use, distribution and reproduction in any medium, provided the original work is properly cited.

DOI: [10.1002/adma.202209633](https://doi.org/10.1002/adma.202209633)

M. Wang, Z. Feng
 School of Chemical, Biological, and Environmental Engineering
 Oregon State University
 Corvallis, OR 97331, USA

P. Tieu
 Department of Chemistry
 University of California, Irvine
 Irvine, CA 92697, USA

M. H. Engelhard
 Environmental Molecular Sciences Laboratory
 Pacific Northwest National Laboratory
 Richland, WA 99354, USA

X. Pan
 Irvine Materials Research Institute (IMRI)
 Department of Physics and Astronomy
 Department of Materials Science and Engineering
 University of California, Irvine
 Irvine, CA 92697, USA

The latest research found that heteroatom adjustment of SACs (via long-range or near-range coordinated interactions) is an effective method to improve the catalytic activities, because of their different electronegativity or atomic radius.^[9] Hence, heteroatoms can adjust the electronic structures and coordination environments of the central metal atoms, thereby changing their analytical properties. For example, Chen et al. included sulfur into Fe–N_x SAC to reduce the energy barrier toward enhanced oxygen evolution and reduction processes under alkaline conditions.^[13] Our group also proposed a chlorine atom adjusted Fe–N₄ SAC to enhance the oxygen reduction activity in H₂–O₂ fuel cells.^[14] Likewise, Zhu and co-workers proposed that by inducing boron (B) to synthesize the B-doped Fe-based SAN, the electronic structure rearrangement of the active iron center can be altered, resulting in significantly enhanced POD-like activity and selectivity.^[15] Ji et al. involved phosphorus (P) heteroatom into Fe–N–C catalysts to form FeN₃P active sites to enhance their POD-like activity via near-range coordinated interactions, and such catalyst can inhibit tumor cell growth effectively.^[9] In this regard, heteroatom adjustment of active sites is an effective method to further improve the catalytic activity of Fe-based SAC and the peroxidase mimicking performance. Although many advances have been made over the years, the different heteroatom adjustments in SACs still needs to optimize heteroatom doping design continuously. It is worth noting that the long-range interaction effect is not like near-range coordinated interactions that can directly affect the

central iron active atom, its mechanism still needs to be further studied and clarified.

In this work, we design and synthesize P-doped 1D carbon nanowires (FeNCP/NWs) with Fe–N₄ active sites. Subsequently, we fully analyze the effect of P modulation to mimic the POD-like activity in response to the need for highly efficient enzyme-like catalysts. To synthesize the FeNCP/NW, 1D polypyrrole nanowire and phytic acid are used as carbon and P sources. Full POD-like activity of the FeNCP/NW and its biosensing applications are validated. Moreover, various structure characterizations as well as mechanism analyses, including chemical strategies and density functional theory (DFT) calculations, are conducted to deeply understand the mechanism of the enhanced activities and specific POD-like properties of FeNCP/NW and the effect of P adjustment.

2. Discussion and Results

DFT calculations were used to investigate the feasibility of the formation of P-doped FeNC SACs with different long-range interaction structures, consisting of single P-atom (Figure S1, Supporting Information)^[16] and double P-atom (Figure S2, Supporting Information) FeN₄C configurations. Their formation energies are calculated and shown in Figure 1a. Our previous work showed that the lowest formation energy of a single P-atom-doped FeN₄C configuration is -776 eV (Figure 1a and

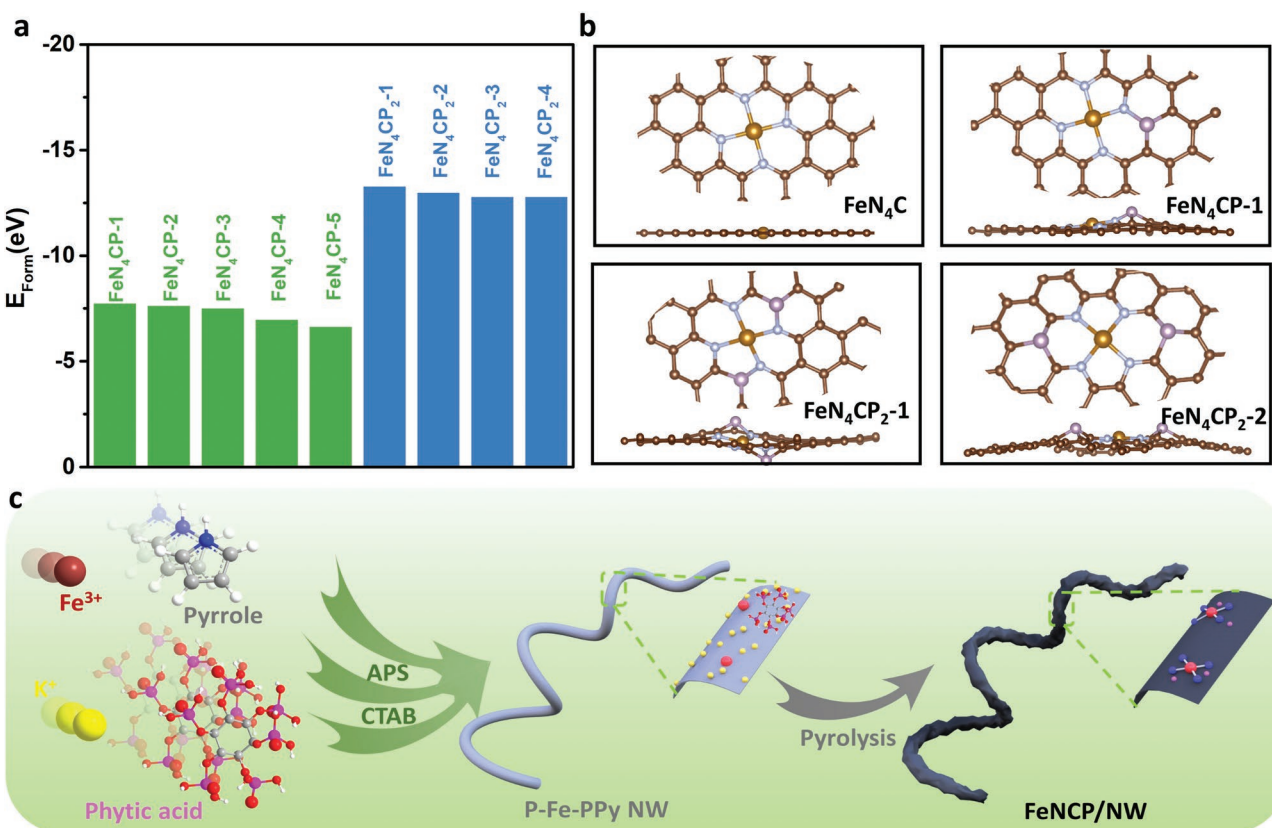


Figure 1. a) The E_{form} of FeNCP/NWs with different P sites and numbers. b) The top and side views of FeN₄C, FeN₄CP-1, FeN₄CP₂-1, and FeN₄CP₂-2 configurations. c) Schematic diagram of the synthesis of FeNCP/NW.

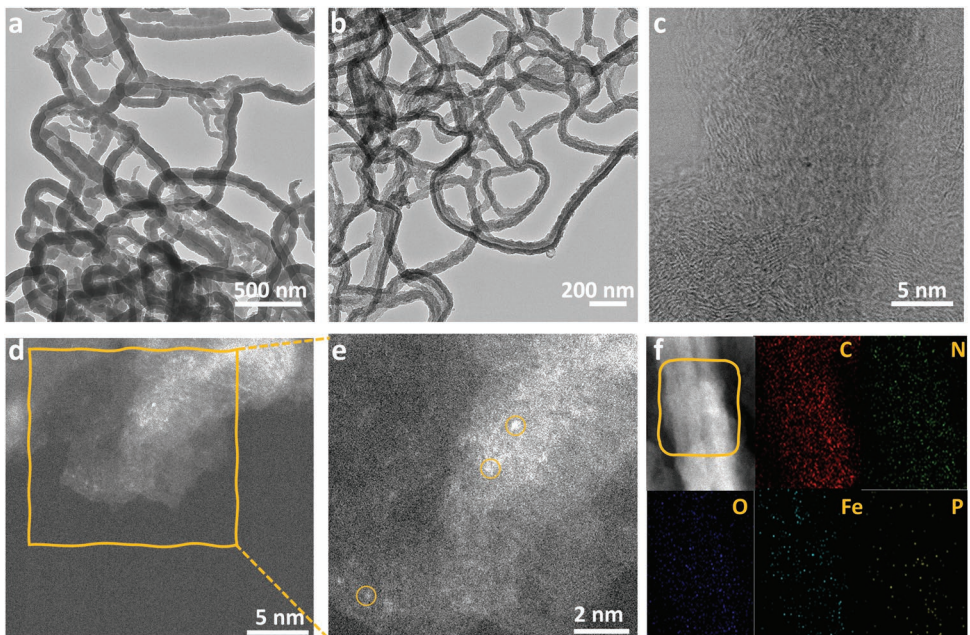


Figure 2. a) TEM image of P–Fe–PPy NW. b) TEM, c) high-magnification BF-STEM, d,e) HAADF-STEM images, and f) the corresponding EDS element mapping image of FeNCP/NW.

Figure S1 (Supporting Information)).^[16] For the double P-atom-doped SACs, configurations of $\text{FeN}_4\text{P}_2\text{-}1$ and $\text{FeN}_4\text{P}_2\text{-}2$ are considered further for POD-like activity, which can be attributed to their more stable formation energy. The specific structures of these most stable configurations and the traditional FeN_4C are shown in Figure 1b. It can be exemplified that the more P atoms are doped into the SAC, the more buckling of the planar SACs is exhibited. This can be explained by the fact that the P atom is larger than C and N atoms in the structure. Hence, while the single and double P-atom-doped SACs appear to be increasingly energetic and stable when considering their formation energies, the overall structure stability decreases as more P atoms are incorporated into the SAC.

The FeNCP/NW is designed based on the secondary-atom-assisted strategy, as well as by adding a certain amount of phytic acid. The potassium ion is used as the secondary atom to reduce the reaction between Fe and P, thereby decreasing the formation of phosphide and the self-aggregating of iron during the pyrolysis process. The specific synthesis process is shown in Figure 1c. Briefly, a complex template was prepared by adding ammonium peroxydisulfate (APS) into a cetyltrimethylammonium bromide (CTAB)/HCl solution. Then, pyrrole, phytic acid, and FeCl_3/KCl (1:20) were added to the above mixture to form a precursor—the P–Fe–polypyrrole nanowires (P–Fe–PPy NWs). Three other kinds of reference Ppy NWs were also synthesized in the same process only without adding phytic acid (Fe–Ppy NWs), metal ions (P–Ppy NWs), as well as phytic acid and FeCl_3/KCl (Ppy NWs), respectively. The carbon catalysts obtained from these NW precursors are FeNC/NW, NCP/NW, and NC/NW, respectively.

Typical 1D nanowire structures can be found in all PPy NW precursors (Figure 2a and Figure S3 (Supporting Information)). After pyrolysis in N_2/NH_3 atmosphere followed by a step of acid washing, 1D nanowire structures of the obtained FeNCP/NW

(Figure 2b), FeNC/NW, NCP/NW, and NC/NW (Figure S4, Supporting Information) are still well-retained. The high-resolution bright-field scanning transmission electron microscopy (BF-STEM) image in Figure 2c shows the distorted graphitic structure of FeNCP/NW. Usually, such a feature can endow enormous specific surface area and rich nanopore structure, where multitudinous P and atomic Fe sites are anchored.^[17] As shown in Figure 2d, high-angle annular dark-field STEM (HAADF-STEM) investigates the structure of FeNCP/NW with intensity differences due to atomic number. The isolated bright spots were identified as single-atomic Fe and circled in yellow, for example (Figure 2e). This finding indicates that plentiful isolated single-atomic Fe sites are hosted on FeNCP/NW. Dispersed Fe atoms are found in the FeNC/NW reference SAC sample, as expected (Figure S7, Supporting Information). Furthermore, energy-dispersive X-ray spectroscopy (EDS) shows that C, N, P, and Fe are uniformly distributed throughout the entire nanowire catalysts (Figure 2f).

The compositions of FeNCP/NW, FeNCP/NW, PNC/NW, and NC/NW were characterized by X-ray photoelectron spectroscopy (XPS). Figure 3a and Figure S8 (Supporting Information) show the high-resolution P 2p of FeNCP/NW and NCP/NW, which are deconvoluted into two peaks at 132.5 and 133.3 eV, which assign to P–C and P–O, respectively.^[18,19] These results demonstrate that P atoms are successfully doped into the carbon matrix. As illustrated in Figure 3b and Figure S9 (Supporting Information), the N 1s XPS spectrum shows that N is present in the form of pyridinic, $\text{Fe}-\text{N}_x$, pyrrolic, graphitic, and oxidized N. Importantly, the FeNCP/NW has a higher $\text{Fe}-\text{N}_x$ percentage (14.9%) than that of the FeNC/NW (11.5%) (Figure 3c), and the Fe content in FeNCP/NW (0.6 at%) is higher than that of FeNC/NW one (0.51 at%). X-ray absorption spectroscopy (XAS) was used further to investigate the Fe atom's chemical states and coordination environment.^[20–22] The Fe K-edge X-ray

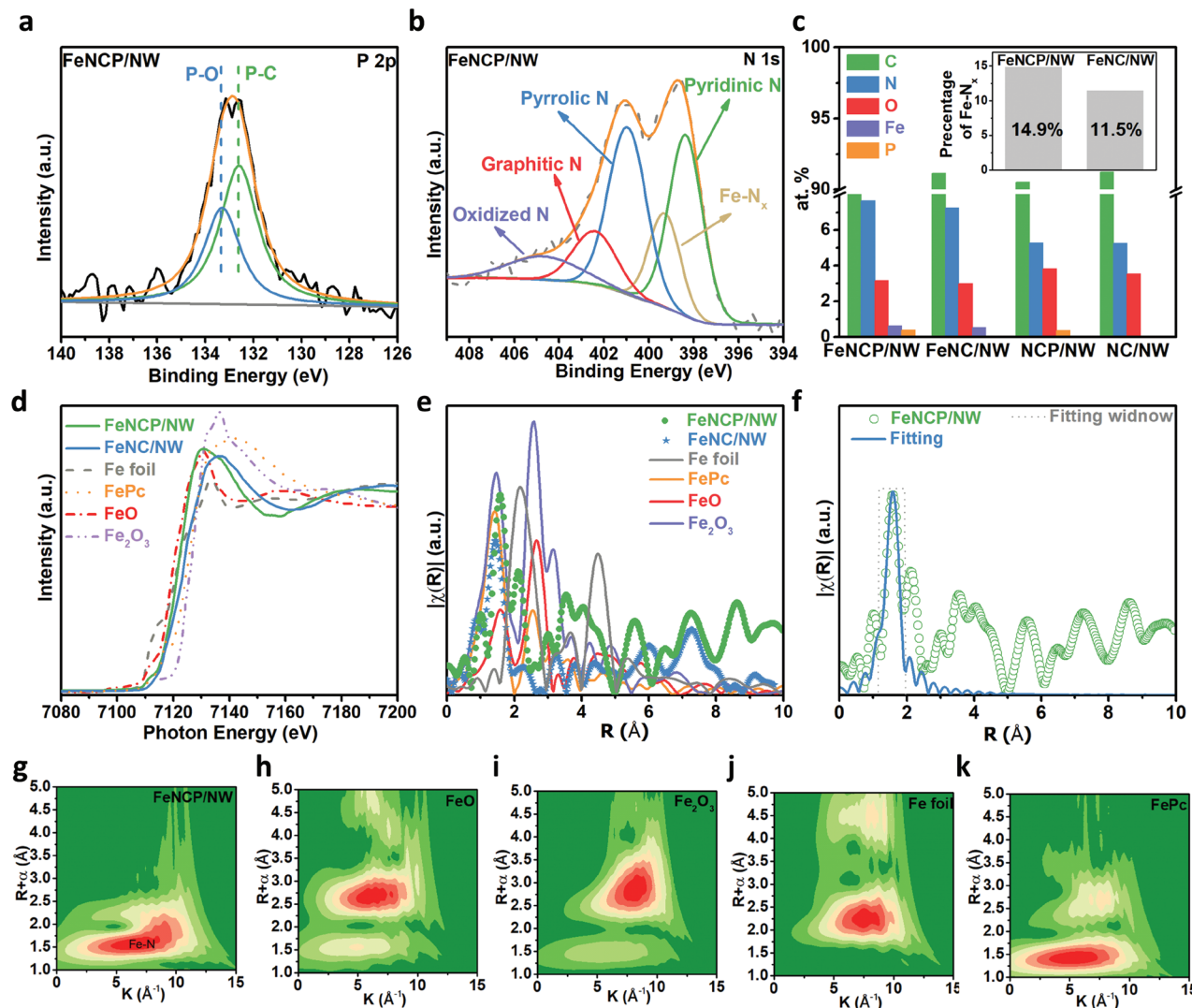


Figure 3. a,b) P 2p and N 1s XPS spectra of FeNCP/NW. c) Element contents of FeNCP/NW, FeNC/NW, FNCP/NW, and NC/NW based on XPS results. The insets show the corresponding percentages of N configurations. d) XANES spectra and e) FT k^2 -weighted EXAFS spectra of FeNCP/NW, FeNC/NW, FePc, Fe foil, FeO, and Fe_2O_3 . f) The corresponding FT-EXAFS fitting curves of the FeNCP/NW in R space and g–k) WT of the FeNCP/NW, FeO, Fe_2O_3 , Fe foil, and FePc, respectively.

absorption near edge structure (XANES) spectra of FeNCP/NW and FeNC/NW are located between FeO and Fe_2O_3 , which means the valence state of Fe is between +2 and +3 (Figure 3d). The energy of FeNCP/NW is lower than FeNC/NW and FePc reference in the rising edge region, which is owing to doped P adjusting the electron density of the Fe center.^[23] From Fourier transforms of extended X-ray absorption fine structure (FT-EXAFS), FeNCP/NW exhibits a strong peak at 1.58 \AA , which is assigned to the Fe–N first coordination shell (Figure 3e).^[24,25] A little Fe crystal signal is found since telling by a small peak at 2.2 \AA is detected. The chemical configuration of single-atom Fe active sites was quantitatively analyzed using FT-EXAFS fitting (Figure 3f and Figure S10 (Supporting Information)). The coordination number of the Fe center in the Fe–N fitting window is around four, and the mean bond length of FeNCP/NW is 2.048 \AA (Table S1, Supporting Information). This result reveals that four N atoms coordinate with Fe atom in

FeNCP/NW, and no P atom has direct interactions with isolated Fe sites. As a result, the doped P should provide long-range interaction with the impact of the Fe active center. Moreover, the Fe K-edge EXAFS oscillations were analyzed by wavelet transform (WT, Figure 3g–k). The WT contour plots show that the maximum at around 6.5 \AA^{-1} is associated with Fe–N.

Typical chromogenic reactions were conducted to evaluate the POD-like activities of all obtained catalysts quantitatively.^[26] The substrate 3,3',5,5'-tetramethylbenzidine (TMB) was used as an electron donor to catalyze the H_2O_2 reduction process.^[27] The absorbance (Figure 4a) and color (Figure S11, Supporting Information) changes show that TMB is oxidized by the FeNCP/NW and FeNC/NW in the presence of H_2O_2 . In comparison, NCP/NW and NC/NW can only trigger negligible color and absorbance changes. The catalytic effect increases with reaction time and shows a linear relation in the first 60 s (Figure 4b). The specific activity of FeNCP/NW reaches 86.9 U mg^{-1} , which

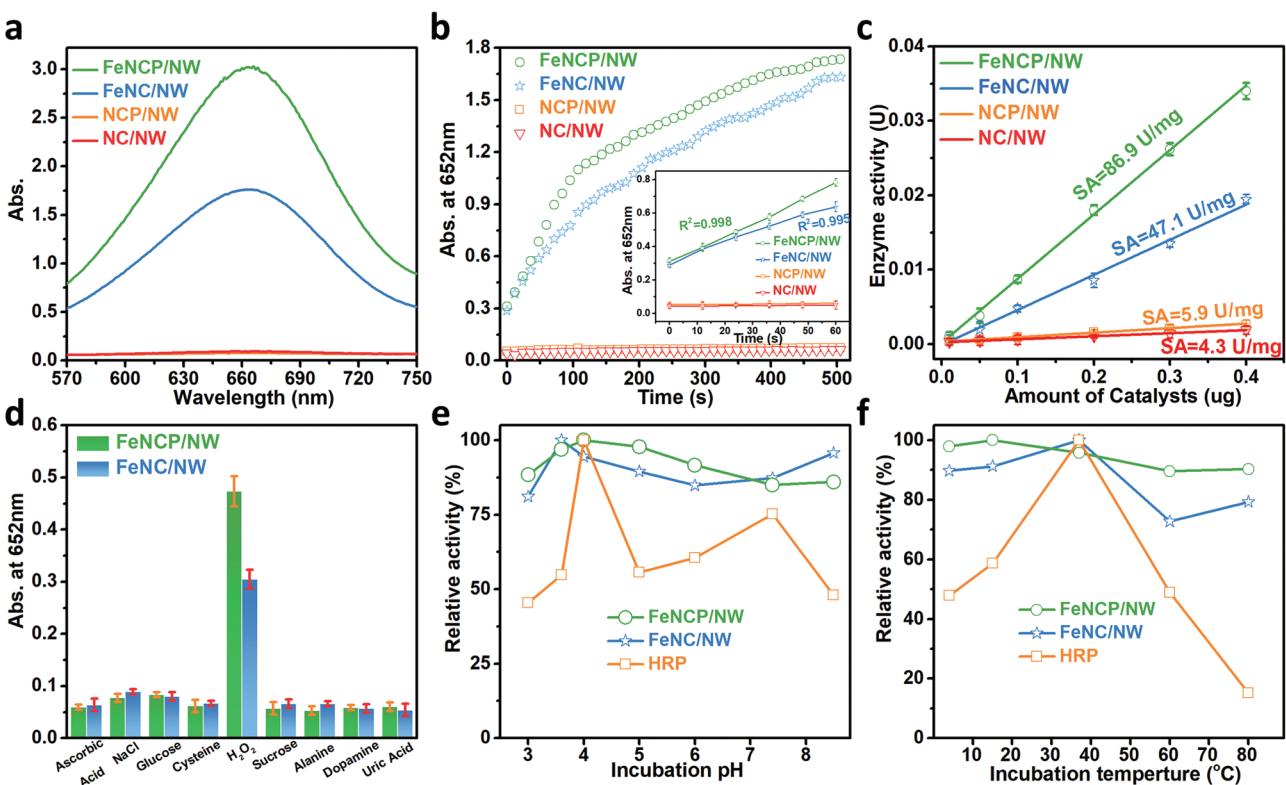


Figure 4. a) Absorption curves, b) absorbance–time curves and magnified initial linear portion of the SAC of TMB chromogenic reaction catalyzed by FeNCP/NW, FeNC/NW, NCP/NW, and NC/NW, respectively. c) Specific activities of synthesized catalysts. d) Selectivity evaluation of FeNCP/NW and FeNC/NW. e,f) Robustness of FeNCP/NW, FeNC/NW, HRP against the harsh environment of temperature and pH, respectively.

is higher than that of reference catalysts (Figure 4c) as well as other reported single-atom iron catalysts (Table S2, Supporting Information). This phenomenon can be attributed to the adjustment of the electronic structure of the Fe active center by P doping. Michaelis–Menten kinetics parameters (Figure S12 and Table S3, Supporting Information) show that FeNCP/NW has a smaller K_m value and better affinity toward TMB and H_2O_2 , even compared with that of natural HRP.^[28] In addition, FeNCP/NW and FeNC/NW display satisfactory selectivities toward H_2O_2 (Figure 4d), similar to the other reported Fe–N–C-based catalysts.^[29] In particular, introducing the P atom improves the catalytic activity without affecting its catalytic specificity. Furthermore, SACs exhibit excellent robustness under harsh pH and high temperature, whereas natural HRP loses its activity, indicating that our SAC has outstanding stability (Figure 4e,f). Also, FeNCP/NW owns a satisfied reproducibility (Figure S13, Supporting Information).

Chemical strategies and theoretical simulation elucidated mechanistic insights into the enhancement of POD-like activity via P atom adjustment. A poisoning experiment using KSCN as a blocking reagent was conducted to detect the most effective section in FeNCP/NW (Figure 5a).^[30,31] The POD-like activity decreased with increasing SCN^- (Figure 5b), which demonstrates that Fe–N₄ sites are the main active sites instead of P sites. And the role of P atoms is supposed to affect the structural or electronic structure of active Fe–N₄ sites. The 5,5-dimethyl-1-pyrroline N-oxide was used as a probe to detect active inter-

mediates by electron spin resonance spectroscopy (Figure S14, Supporting Information), and strong signal responses are assigned to $\cdot OH$.^[32] The detected small peaks mean little other reactive oxygen species (ROS) existed, which is owing to the other enzyme-like (oxidase-like, superoxide dismutase-like, etc.) activities of Fe–N–C catalysts.^[15,33] Various scavengers (Na₃N, isopropanol, thiourea, and β -carotene) were used to trap ROS ($\cdot OH$ / O_2^- , $\cdot OH$, and 1O_2).^[34] The inhibition effects are significantly enhanced after continuously increasing the concentration of scavengers (Figure 5c–f). These results reveal that ROS are the main active intermediate to oxide TMB.

DFT calculations were performed to understand better the mechanism and effect of the P adjustment on POD-like activity. The most stable configurations from Figure 1b were chosen here to calculate their activities further. The bond length of Fe–O (1.825 Å) on FeN₄CP-1 is shorter than that of others (Figure 5g). This suggests that the FeN₄CP-1 structure has the strongest binding ability to O species. According to the energy diagram shown in Figure 5h, the FeN₄CP-1 model has the lowest energy barrier for generating a reactive hydroxyl radical and an adsorbed hydroxyl group, indicating that the single P-dopant FeN₄C model is energetically more favorable for the reaction process of hydroxyl radical generation. Löwdin charge analysis was performed on several SACs with variable P-dopant concentrations, where the given values are the change in Löwdin charge from the SACs with $\cdot OH$ adsorbed and the SAC with a bare surface. Table S4 (Supporting Information) shows that

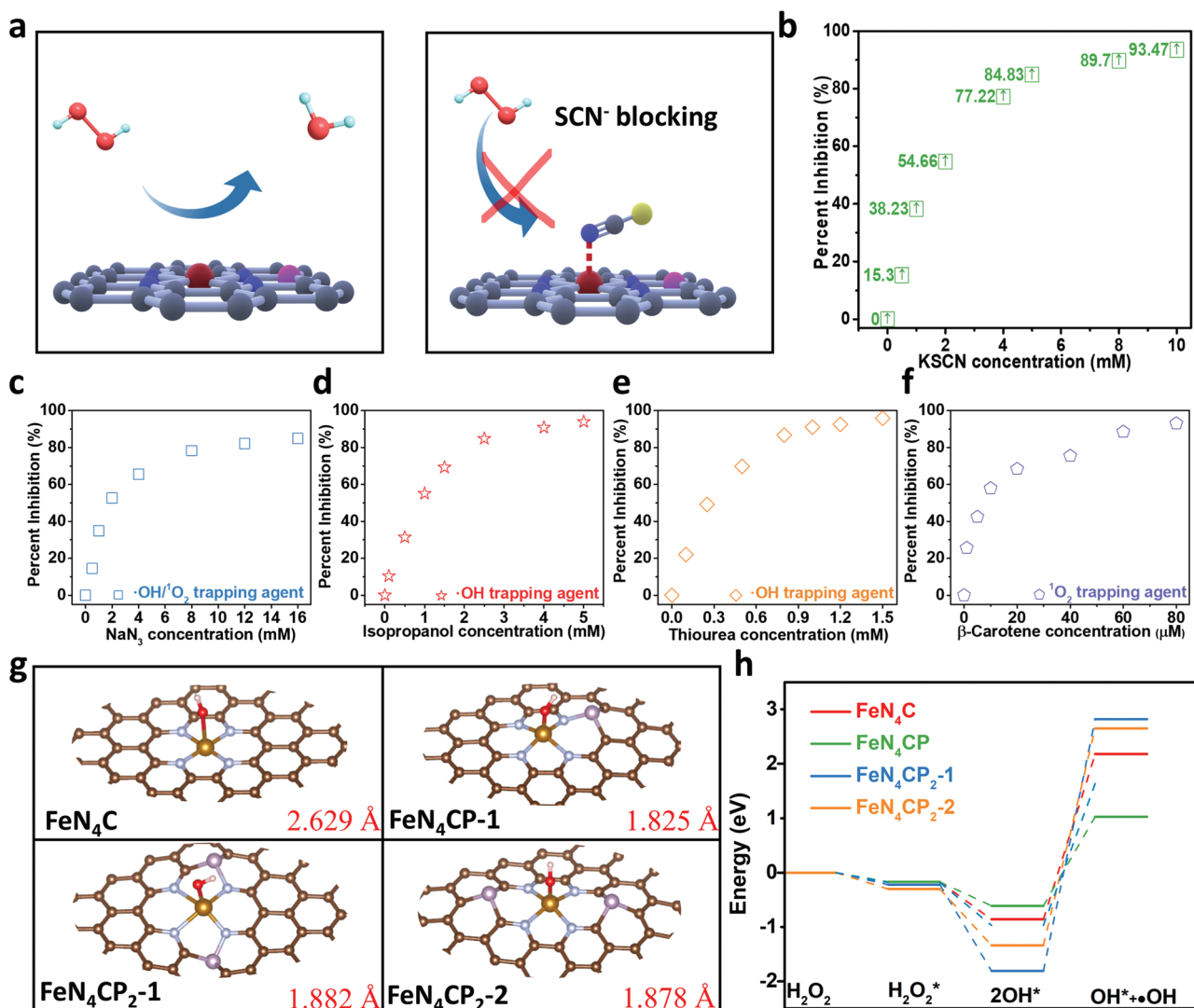


Figure 5. a) Schematic illustration of the mechanism of the POD-like catalytic process and the KSCN influence. Gray balls: C; blue: N; wine: Fe; pink: P; red: O; cyan: H. b–f) Percent inhibition after adding KSCN, Na₃, isopropanol, thiourea, and β-carotene, respectively. g) The Fe–O bond distances of Fe₄N₂C, Fe₄N₂CP-1, Fe₄N₂CP₂-1, and Fe₄N₂CP₂-2 configurations. h) Energy diagram of the POD-like reaction process for calculated models.

there is a considerable rise in Fe from the undoped SAC to the P-doped SAC. The addition of the P-dopant leads to a significant decrease in the change of Löwdin charge for N. As a result, the P-dopant causes an increase in the change of Löwdin charge for the Fe atom, suggesting the increased interaction between the Fe and O atom. This is facilitated by the decrease in charge associated with the N atom as the P-dopant is introduced. However, the change in Löwdin charge for the P atom is observed to be insignificant as its concentration in the SAC increases. Thus, little P addition allows the Fe atom to be more active for catalytic activity, but raising the P amount cannot benefit further. Such mechanism analysis also correlated to the POD-like activities in various quantities of P-adjusted FeNCP/NW. As shown in Figure S15 (Supporting Information), the POD-like activity is increased while adding the P source in the synthesis step. Nevertheless, the POD-like activity is decreased gradually while continuously adding the amount of P.

As a proof-of-principle application, FeNCP/NW was used in an enzyme-cascade sensing platform for colorimetric acetylcholine (ACh) sensing. ACh is an important neurotransmitter in both peripheral and central nervous systems, as well as a biomarker for various neurological diseases, like Parkinson's disease, Alzheimer's disease, schizophrenia, etc.^[35] It is crucial to analyze ACh accurately with high sensitivity and match the disease diagnosis requirements. The sensing principle of the enzyme-cascade platform is shown in Figure 6a. Specifically, the ACh can be catalyzed into choline (Ch) by acetylcholinesterase (AChE), and thereby produce H₂O₂ under the oxygen and choline oxidase (ChOx) conditions.^[36,37] Then, the excellent POD-like activity of FeNCP/NW endows it to detect ACh with high sensitivity. The results shown in Figure 6b further confirm the sensing mechanism. No or little absorbance is observed under individual ACh, AChE, and ACh + AChE. In Figure 6c, the intensity of UV-vis absorbance increases gradually with the

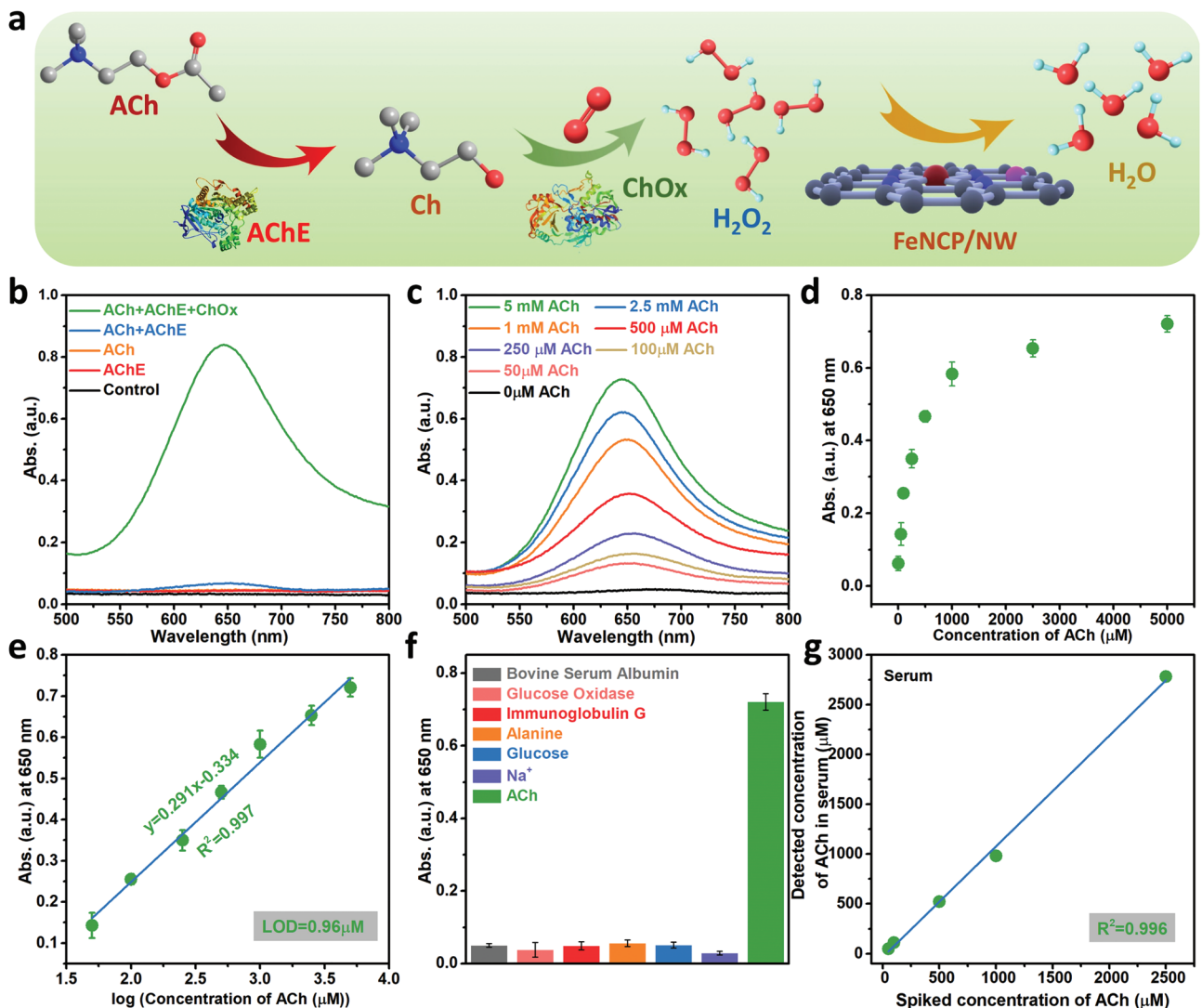


Figure 6. a) Schematic illustration of the ACh sensing process of the AChE/ChOx/FeNCP/NW cascade platform. b) Absorption curves of the FeNCP/NW + TMB in solutions of AChE, ACh, ACh + AChE, ACh + AChE + ChOx, and control solutions, respectively. c,d) Absorption curves and optical density (OD) values at 650 nm of different concentrations of ACh in the AChE/ChOx/FeNCP/NW cascade platform, respectively. e) The linear calibration response for ACh. f) Absorption values of the AChE/ChOx/FeNCP/NW cascade platform with different targets. g) Comparison of spiked and detected ACh levels in human serum.

ACh concentration enhancement. Their specific absorbance values at 652 nm are shown in Figure 6d. The linear relationships of ACh concentrations and their absorbance values from 50 μM to 5 mM were established in Figure 6e, which has a detection limit of 0.96 μM. Such a high sensitivity toward ACh is also better than other reported nanomaterial-based ACh biosensing works, including single-atom-based,^[38] precious-metal-based,^[39] transition-metal-based,^[40] quantum dots,^[41] and more summarized in Table S5 (Supporting Information). Additionally, the outstanding selectivity (Figure 6f), anti-interference ability (Figure S16, Supporting Information), and recovery test results (Figure 6g and Table S6 (Supporting Information)) further demonstrated the potential practical biosensing abilities. The glucose oxidase–FeNCP/NW sensing platform further demonstrates their excellent practical sensing ability (Figure S17 and Table S7, Supporting Information).

3. Conclusion

We successfully synthesized a novel phosphorus-doped single-atom Fe nanowire (FeNCP/NW) in this work. Phytic acids are utilized as the phosphorus source for the P doping in FeNCP/NW synthesis. The results demonstrate that FeNCP/NW has remarkable POD-like activity, exceptional selectivity, and good stability. The EXAFS characterizations, scavenger analysis, and DFT calculations indicated that the Fe site is the primary activity center and revealed the mechanism of phosphorus modulation for the increased POD-like activity. Introducing P in SAC can first enhance POD-like activity greatly, however, this effect becomes insignificant if continuously involving too much of P. Finally, FeNCP/NW was applied in an enzyme-cascade sensor platform for colorimetric ACh sensing. A wide sensing regime spanning from 50 μM to 5 mM with detection limit of 0.96 μM

was achieved. This work paves a new way for creating high-performance enzyme-like SACs with boosted catalytic activity, which can replace natural enzymes in a variety of biomedical applications, including immunoassay, cancer treatment, wound repair, and various bioimaging.

Supporting Information

Supporting Information is available from the Wiley Online Library or from the author.

Acknowledgements

This work was supported by a GAP fund from the Washington State University. This work used resources of the WSU Franceschi Microscopy & Imaging Center for TEM measurements, and the XPS was performed using EMSL (Grant No. grid.436923.9), a DOE Office of Science User Facility sponsored by the Office of Biological and Environmental Research. XAS measurements, supported by the U.S. National Science Foundation (Grant No. CBET-1949870), were done at 9-BM of Advanced Photon Source, a US DOE Office of Science user facility operated for the US DOE by the Argonne National Laboratory, which is supported by DOE under Grant No. DE-AC02-06CH11357. The work at UC Irvine was supported by the National Science Foundation (NSF) awards under Grant Nos. CHE-1955786 and CBET-2031494. J.A.B. acknowledges the financial support by the National Science Foundation Graduate Research Fellowship under Grant No. DGE1255832. Computational resources were provided by the high-performance computing cluster Kamiak located at the Washington State University.

Conflict of Interest

The authors declare no conflict of interest.

Data Availability Statement

The data that support the findings of this study are available from the corresponding author upon reasonable request.

Keywords

biosensing, Fe–N–C, heteroatoms, nanozymes, peroxidase mimicking, single-atom catalysts

Received: October 19, 2022

Revised: December 7, 2022

Published online: March 13, 2023

- [1] B. Qiao, A. Wang, X. Yang, L. F. Allard, Z. Jiang, Y. Cui, J. Liu, J. Li, T. Zhang, *Nat. Chem.* **2011**, *3*, 634.
- [2] Y. Chen, S. Ji, C. Chen, Q. Peng, D. Wang, Y. Li, *Joule* **2018**, *2*, 1242.
- [3] C. Zhu, S. Fu, Q. Shi, D. Du, Y. Lin, *Angew. Chem., Int. Ed.* **2017**, *56*, 13944.
- [4] L. Huang, J. Chen, L. Gan, J. Wang, S. Dong, *Sci. Adv.* **2019**, *5*, eaav5490.
- [5] L. Jiao, H. Yan, Y. Wu, W. Gu, C. Zhu, D. Du, Y. Lin, *Angew. Chem., Int. Ed.* **2020**, *59*, 2565.

- [6] L. Jiao, J. Wu, H. Zhong, Y. Zhang, W. Xu, Y. Wu, Y. Chen, H. Yan, Q. Zhang, W. Gu, L. Gu, S. P. Beckman, L. Huang, C. Zhu, *ACS Catal.* **2020**, *10*, 6422.
- [7] H. Xiang, W. Feng, Y. Chen, *Adv. Mater.* **2020**, *32*, 1905994.
- [8] S. Ding, Z. Lyu, L. Fang, T. Li, W. Zhu, S. Li, X. Li, J.-C. Li, D. Du, Y. Lin, *Small* **2021**, *17*, 2100664.
- [9] S. Ji, B. Jiang, H. Hao, Y. Chen, J. Dong, Y. Mao, Z. Zhang, R. Gao, W. Chen, R. Zhang, Q. Liang, H. Li, S. Liu, Y. Wang, Q. Zhang, L. Gu, D. Duan, M. Liang, D. Wang, X. Yan, Y. Li, *Nat. Catal.* **2021**, *4*, 407.
- [10] L. Jiao, W. Xu, Y. Wu, H. Yan, W. Gu, D. Du, Y. Lin, C. Zhu, *Chem. Soc. Rev.* **2021**, *50*, 750.
- [11] C.-B. Ma, Y. Xu, L. Wu, Q. Wang, J.-J. Zheng, G. Ren, X. Wang, X. Gao, M. Zhou, M. Wang, H. Wei, *Angew. Chem., Int. Ed.* **2022**, *61*, e202116170.
- [12] Z. Lyu, S. Ding, N. Zhang, Y. Zhou, N. Cheng, M. Wang, M. Xu, Z. Feng, X. Niu, Y. Cheng, C. Zhang, D. Du, Y. Lin, *Research* **2020**, *2020*, 4724505.
- [13] P. Chen, T. Zhou, L. Xing, K. Xu, Y. Tong, H. Xie, L. Zhang, W. Yan, W. Chu, C. Wu, Y. Xie, *Angew. Chem., Int. Ed.* **2017**, *56*, 610.
- [14] S. Ding, J. A. Barr, Q. Shi, Y. Zeng, P. Tieu, Z. Lyu, L. Fang, T. Li, X. Pan, S. P. Beckman, D. Du, H. Lin, J.-C. Li, G. Wu, Y. Lin, *ACS Nano* **2022**, *16*, 15165.
- [15] L. Jiao, W. Xu, Y. Zhang, Y. Wu, W. Gu, X. Ge, B. Chen, C. Zhu, S. Guo, *Nano Today* **2020**, *35*, 100971.
- [16] J.-C. Li, H. Zhong, M. Xu, T. Li, L. Wang, Q. Shi, S. Feng, Z. Lyu, D. Liu, D. Du, S. P. Beckman, X. Pan, Y. Lin, M. Shao, *Sci. China Mater.* **2020**, *63*, 965.
- [17] M. Xiao, J. Zhu, L. Ma, Z. Jin, J. Ge, X. Deng, Y. Hou, Q. He, J. Li, Q. Jia, S. Mukerjee, R. Yang, Z. Jiang, D. Su, C. Liu, W. Xing, *ACS Catal.* **2018**, *8*, 2824.
- [18] G. Hasegawa, T. Deguchi, K. Kanamori, Y. Kobayashi, H. Kageyama, T. Abe, K. Nakanishi, *Chem. Mater.* **2015**, *27*, 4703.
- [19] F. Razmjooei, K. P. Singh, D.-S. Yang, W. Cui, Y. H. Jang, J.-S. Yu, *ACS Catal.* **2017**, *7*, 2381.
- [20] M. Wang, Z. Feng, *Curr. Opin. Electrochem.* **2021**, *30*, 100803.
- [21] M. Wang, Z. Feng, *Chem. Commun.* **2021**, *57*, 10453.
- [22] M. Wang, L. Árnadóttir, Z. J. Xu, Z. Feng, *Nano-Micro Lett.* **2019**, *11*, 47.
- [23] X. Zhang, Y. Wang, M. Gu, M. Wang, Z. Zhang, W. Pan, Z. Jiang, H. Zheng, M. Lucero, H. Wang, G. E. Sterbinsky, Q. Ma, Y.-G. Wang, Z. Feng, J. Li, H. Dai, Y. Liang, *Nat. Energy* **2020**, *5*, 684.
- [24] X. Zeng, J. Shui, X. Liu, Q. Liu, Y. Li, J. Shang, L. Zheng, R. Yu, *Adv. Energy Mater.* **2018**, *8*, 1701345.
- [25] J. Wang, S. Yin, Q. Zhang, F. Cao, Y. Xing, Q. Zhao, Y. Wang, W. Xu, W. Wu, M. Wu, *J. Catal.* **2021**, *404*, 89.
- [26] B. Jiang, D. Duan, L. Gao, M. Zhou, K. Fan, Y. Tang, J. Xi, Y. Bi, Z. Tong, G. F. Gao, N. Xie, A. Tang, G. Nie, M. Liang, X. Yan, *Nat. Protoc.* **2018**, *13*, 1506.
- [27] L. Jiao, Y. Kang, Y. Chen, N. Wu, Y. Wu, W. Xu, X. Wei, H. Wang, W. Gu, L. Zheng, W. Song, C. Zhu, *Nano Today* **2021**, *40*, 101261.
- [28] X. Niu, Q. Shi, W. Zhu, D. Liu, H. Tian, S. Fu, N. Cheng, S. Li, J. N. Smith, D. Du, Y. Lin, *Biosens. Bioelectron.* **2019**, *142*, 111495.
- [29] Z. Lyu, S. Ding, M. Wang, X. Pan, Z. Feng, H. Tian, C. Zhu, D. Du, Y. Lin, *Nano-Micro Lett.* **2021**, *13*, 146.
- [30] J. Masa, W. Xia, M. Muhler, W. Schuhmann, *Angew. Chem., Int. Ed.* **2015**, *54*, 10102.
- [31] Z. Li, Y. Chen, S. Ji, Y. Tang, W. Chen, A. Li, J. Zhao, Y. Xiong, Y. Wu, Y. Gong, T. Yao, W. Liu, L. Zheng, J. Dong, Y. Wang, Z. Zhuang, W. Xing, C.-T. He, C. Peng, W.-C. Cheong, Q. Li, M. Zhang, Z. Chen, N. Fu, X. Gao, W. Zhu, J. Wan, J. Zhang, L. Gu, S. Wei, et al., *Nat. Chem.* **2020**, *12*, 764.
- [32] Y. Zhao, X. Xiao, M. Zou, B. Ding, H. Xiao, M. Wang, F. Jiang, Z. Cheng, P. Ma, J. Lin, *Adv. Mater.* **2021**, *33*, 2006363.

- [33] Y. Wu, L. Jiao, X. Luo, W. Xu, X. Wei, H. Wang, H. Yan, W. Gu, B. Z. Xu, D. Du, Y. Lin, C. Zhu, *Small* **2019**, *15*, 1903108.
- [34] Y. Zhan, Y. Zeng, L. Li, L. Guo, F. Luo, B. Qiu, Y. Huang, Z. Lin, *Anal. Chem.* **2020**, *92*, 1236.
- [35] E. Ö. Bolat, G. A. Tiğ, Ş. Pekyardımcı, *J. Electroanal. Chem.* **2017**, *785*, 241.
- [36] D. Kong, R. Jin, X. Zhao, H. Li, X. Yan, F. Liu, P. Sun, Y. Gao, X. Liang, Y. Lin, G. Lu, *ACS Appl. Mater. Interfaces* **2019**, *11*, 11857.
- [37] S. Hou, Z. Ou, Q. Chen, B. Wu, *Biosens. Bioelectron.* **2012**, *33*, 44.
- [38] Y. Wu, J. Wu, L. Jiao, W. Xu, H. Wang, X. Wei, W. Gu, G. Ren, N. Zhang, Q. Zhang, L. Huang, L. Gu, C. Zhu, *Anal. Chem.* **2020**, *92*, 3373.
- [39] S.-B. He, G.-W. Wu, H.-H. Deng, A.-L. Liu, X.-H. Lin, X.-H. Xia, W. Chen, *Biosens. Bioelectron.* **2014**, *62*, 331.
- [40] L. Su, X. Yu, W. Qin, W. Dong, C. Wu, Y. Zhang, G. Mao, S. Feng, *J. Mater. Chem. B* **2017**, *5*, 116.
- [41] Z. Chen, X. Ren, X. Meng, D. Chen, C. Yan, J. Ren, Y. Yuan, F. Tang, *Biosens. Bioelectron.* **2011**, *28*, 50.